# A Hybrid RANS-LES Dataset for Data-Driven Turbulent Mean Flow Reconstruction


**Omid Bidar, Sean R Anderson, and Ning Qin**

**Abstract** This paper presents results for a set of parameterised periodic hill geometries using the hybrid RANS-LES approach based on the Spalart-Allmaras improved delayed-detached eddy simulation (IDDES). These results are compared with data from direct numerical simulations. The dataset is intended to be used for data-driven Reynolds-averaged Navier-Stokes (RANS) closure modelling for aerodynamic shape optimisation. As a demonstration, the IDDES data for the baseline geometry is used for turbulent mean flow reconstruction with the $k - \omega$ shear stress transport model. Flow reconstruction results demonstrate considerable improvements compared to the baseline RANS model.

## 1 Introduction

Data-driven flow simulations and/or analyses are an active research pursuit in the fluid dynamics community. While the research breadth is very broad–e.g. enhanced reduced order modelling through dynamic mode decomposition [2], physics-informed neural networks [3], turbulence closure modelling [1] etc.–this paper presents the first step towards exploring data-driven turbulence closure modelling in the context of aerodynamic shape optimisation. Our final goal is to study the deep learning-enhancement of turbulence models in the contexts of Reynolds-averaged Navier-Stokes (RANS) simulations when performing aerodynamic shape

CUFS-2024-7, Cambridge, United Kingdom, 4-5 March 2024.

O. Bidar (✉)
University of Sheffield, Sheffield, England
e-mail: obidar1@sheffield.ac.uk

S. R. Anderson
School of Electrical and Electronic Engineering, University of Sheffield, Sheffield, England
e-mail: s.anderson@sheffield.ac.uk

N. Qin
School of Mechanical, Aerospace and Civil Engineering, University of Sheffield, Sheffield, England
e-mail: n.qin@sheffield.ac.uk



J. C. Tyacke and N. R. Vadlamani (eds.), *Proceedings of the Cambridge Unsteady Flow Symposium 2024*, https://doi.org/10.1007/978-3-031-69035-8_7

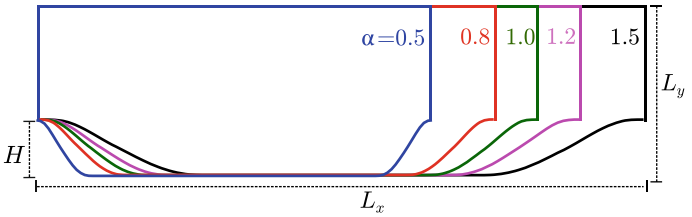


**Fig. 1** Parameterised periodic hill geometries for generating the training dataset

optimisation in complex flow conditions–where existing turbulence closures are prone to inaccuracies. To that end, here we present a training dataset for a set of parameterised periodic hills, generated using hybrid RANS-LES simulations. This approach is especially appealing in high Reynolds number aerodynamic flows such as those encountered in the aerospace industry, since the computational resources requirement is much lower than large eddy or direct numerical simulations.

In aerodynamic shape optimisation, many flow simulations are required to iteratively find the optimal shape, which largely restricts the highest level of fidelity in terms of turbulence modelling to RANS-based simulations due computational resources required. While potentially adequate in on-design scenarios, e.g. wing optimisation in steady, level flight, the accuracy in flow predictions can become problematic in more complex settings, e.g. wing near stall, where complex flow phenomena such as separation due to adverse pressure gradients is poorly predicted by RANS-based turbulence models. Recent advances in machine-learning based augmentation of turbulence models for such complex flows have inspired us to investigate their application in aerodynamic shape optimisation to address the aforementioned challenges in existing RANS-based approaches.

In order to investigate the potential of machine learning in enhanced turbulence modelling for aerodynamic shape optimisation a dataset of high-fidelity data is required. As a proof-of-concept we selected the periodic hill case, with the parameterisation by Xiao *et al.* [4], shown in Fig. 1. The original periodic hill case ($\alpha = 1.0$ in Fig. 1) is a simple geometry that features flow separation due to the curved surface, and flow reattachment on a flat plate. Additionally, this case has well-defined boundary conditions, and relatively affordable computational cost. As the analysis of separated flows over curved surfaces is a common characteristic of many practical application, the periodic hill case is a popular benchmark case for high-order simulations (LES and DNS), and evaluation of RANS turbulence models. Breuer *et al.* [5] performed detailed numerical simulations using DNS and highly-resolved LES, with comparisons against PIV experimental measurements up to $Re = 10{,}595$. Rapp and Manhart performed experimental measurements up to $Re = 37{,}000$ [32]. Other examples of numerical simulations include: [6, 21] (DNS), [7, 21, 22] (LES), and [23, 29–31] (hybrid RANS-LES).

While mean DNS fields for the set of geometries in Fig. 1 are available, we choose to generate our own dataset using hybrid RANS-LES methods. The reasons for this are two-fold: aerodynamic shape optimisation is generally performed where the goal is to optimise wall-quantities (e.g. minimising surface drag coefficient/skin friction), however, the aforementioned dataset does not provide these to benchmark the RANS-based predictions; secondly, after shape optimisation is performed using the machine learning-enhanced turbulence model, the flow predictions for the optimised shape must be validated using the higher-fidelity simulations used to generate the training data. Therefore, in order to have full access to all quantities of interest, and a consistent high-fidelity simulation setup for the training and validation data–while avoiding excessive computational requirements in DNS–we generate the data using improved-delayed detached-eddy simulations (IDDES). The available quantities from the DNS dataset will be used to verify our IDDES results.

Many approaches to utilising data assimilation and machine learning techniques for RANS-based turbulence modelling have been introduced over the past decade. These include: generating data-driven Reynolds stress model closures using novel neural network architectures with embedded invariance properties [8]; formulating algebraic nonlinear closures using gene expression programming and symbolic regression [9, 10]; using data for uncertainty quantification, and many more, comprehensively reviewed in the following papers: [1, 11].

Our overall goals in this research is to explore field inversion and machine learning[12, 13]. In the paper the focus is the former step, i.e. field inversion. The field inversion step involves perturbation of the transport equation(s) for an existing turbulence model, and the solution of multiple inverse problems (for varying flow conditions and/or geometries) to reconstruct turbulent mean flow given the high-fidelity data. Field inversion-based flow reconstruction is case specific, i.e. it cannot be used for prediction of flows outside the training dataset. Therefore, machine learning approaches such as deep neural networks (e.g. [12]) or Gaussian processes (e.g. [13]) are used to generalise the model corrections for flow conditions/geometries beyond—but similar to—the training dataset. Benefits of the FIML approach are model-consistency, and the ability to work with relatively sparse data, e.g. [12, 14]. We stress, this paper will only present field inversion results, while the machine learning generalisation is the subject of ongoing work.

The rest of the paper is structured as follows: in Sect. 2 we introduce the IDDES methodology and compare the results against the DNS data; in Sect. 3 we introduce the field inversion approach for turbulent mean flow reconstruction and present the results for the baseline shape ($\alpha = 1.0$); and finally the paper is concluded with an outline of future work in Sect. 4.

## 2 IDDES Dataset

Hybrid methods utilise a closure model in the near-wall region of the flow, while performing eddy-resolving simulation away from the wall. The predictions with these

methods can be significantly more accurate than RANS models, while requiring a coarser mesh than required for wall-resolved LES, or DNS [15, 16]. In this work we use the Spalart-Allmaras IDDES model [17], outlined in the Appendix, to generate the dataset for the parameterised periodic hills.

## 2.1 Periodic Hill Flow Simulation Overview

The periodic hill flow is driven by a constant pressure gradient which is established by adding a source term in the momentum equation. The Reynolds number, $Re_H = 5,600$ for all the parameterised geometries in Fig. 1, is defined as follows:

$$Re_H = \frac{U_b H}{\nu}, \qquad U_b = \frac{1}{2.035H} \int_H^{3.035H} U_x(y)\, dy, \tag{1}$$

where $U_b$ is the bulk velocity, $\nu$ is the kinematic viscosity, and $U_x$ is the streamwise velocity component.

Cyclic boundary conditions are applied at the inlet, outlet, and the spanwise directions, while no-slip is imposed at the hills and top wall. Two different mesh resolutions are used. For $\alpha = \{0.5, 0.8, 1.0\}$ the number of cells is $n_x \times n_y \times n_z = 200 \times 160 \times 80 = 2.56 \times 10^6$, while for $\alpha = \{1.2, 1.5\}$, the number of cells is $n_x \times n_y \times n_z = 400 \times 220 \times 80 = 7.04 \times 10^6$. The mesh are deliberately dense to reduce mesh related inaccuracies. The geometry in the spanwise direction is extended by half the streamwise length of the baseline geometry, i.e. $L_z = 9H/2$ following the DNS dataset. The time-step used is $\Delta t = 0.0004$, and the data is collected over a time period of $T = 350H/U_b$.

The simulations are run in OpenFOAM [26], based on the finite-volume method. The convective term in the momentum equation is discretised using the hybrid scheme of Travin *et al.* [27] blending a second-order central difference scheme for the LES regions, and a second-order upwind scheme for the RANS regions. All other terms were discretised using a second-order limited linear differencing scheme. The PIMPLE algorithm is used for the pressure-velocity coupling, which combines the Pressure-Implicit with Splitting of Operators (PISO) and the Semi-Implicit Method for Pressure Linked Equations (SIMPLE) algorithms [28].

## 2.2 Results and Comparison to DNS

The IDDES results—averaged over time and space in the spanwise ($z$-axis) direction—will be compared against the DNS data from Xiao *et al.* [4] and some commonly used RANS-based turbulence models implemented in OpenFOAM: $k - \epsilon$ [25], Menter $k - \omega$ [24], and $k - \omega$ SST [20]. For brevity, the focus will be on the baseline periodic hill geometry ($\alpha = 1.0$). The streamwise and wall-normal velocity

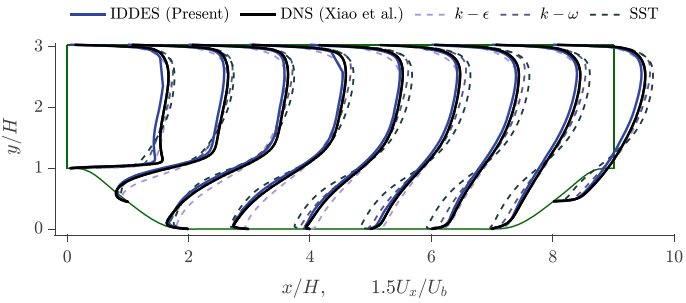


**Fig. 2** Comparison of the streamwise velocity profiles

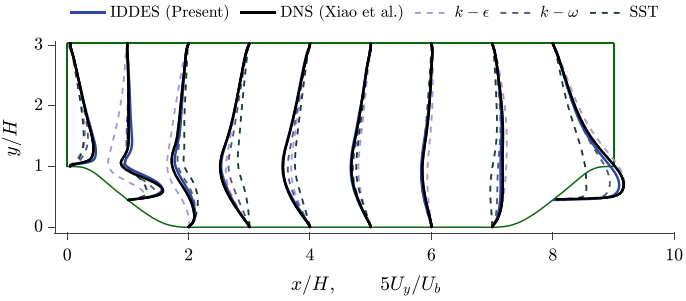


**Fig. 3** Comparison of the wall-normal velocity profiles

profiles comparisons are shown in Figs. 2 and 3, respectively. The IDDES results agree well with the DNS reference, while there are discrepancies in all the RANS models considered. The most significant errors in the RANS models are present in separation zone after the first hill crest.

Similarly, profiles of normal and shear Reynolds stresses are shown in Figs. 4 and 5, respectively. It is clear that the IDDES is largely able to match the DNS data, while all the RANS models show significant inaccuracies, especially in the normal Reynolds stress predictions. Figure 6 shows the skin friction predictions. As Xiao *et al.* [4] dataset does not provide wall quantities, we use the DNS data by Krank *et al.* [6] as surrogate. Again, IDDES result closely match the reference data, while the RANS models fail to accurately capture the flow separation and re-attachment, especially, in the case of $k-\epsilon$ and $k-\omega$ SST models, which significantly under-predict or over-predict the size of the separation zone, respectively.

Figure 7 compares the drag coefficient prediction on the hill wall for the different geometries, with the different models. It is clear that the drag rises as the hill crests become steeper. This is due to the higher flow separation, as illustrated in the sizes of the recirculation zones for the steepest ($\alpha = 0.5$) and shallowest ($\alpha = 1.5$) hill geometries, in Fig. 8. The RANS-based drag predictions are higher than the IDDES results, considerably so in the case of $k-\epsilon$ and the $k-\omega$ model.

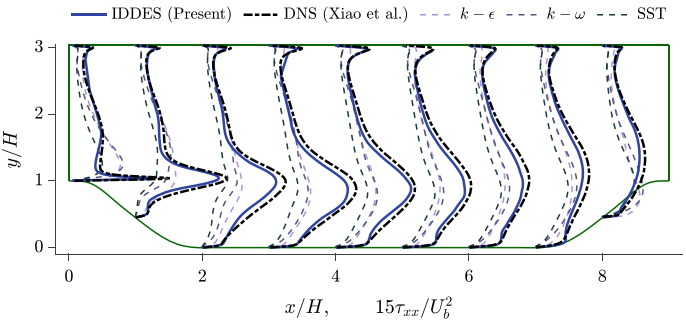


**Fig. 4** Comparison of the normal Reynolds stress profiles

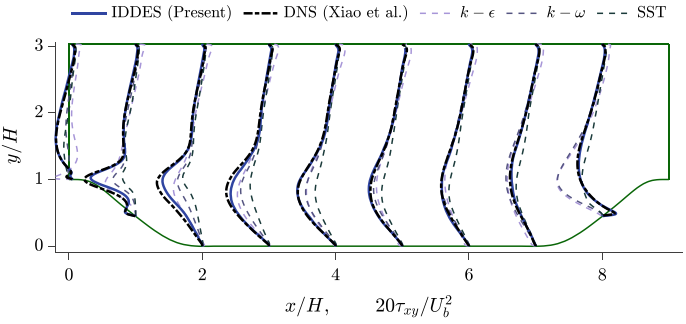


**Fig. 5** Comparison of the Reynolds shear stress profiles

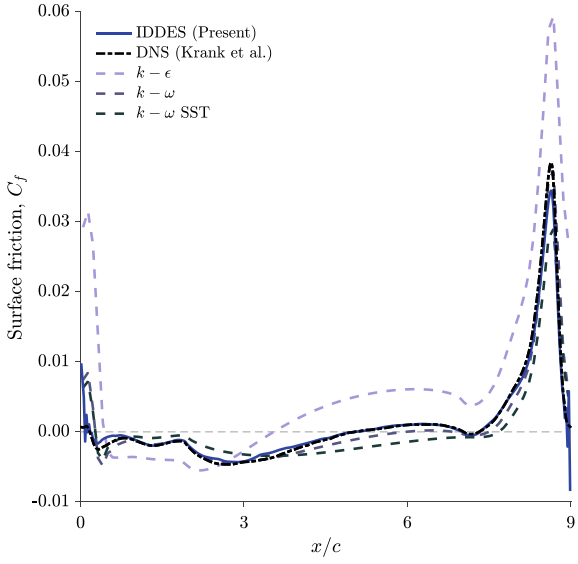


**Fig. 6** Comparison of the skin friction on the hill wall

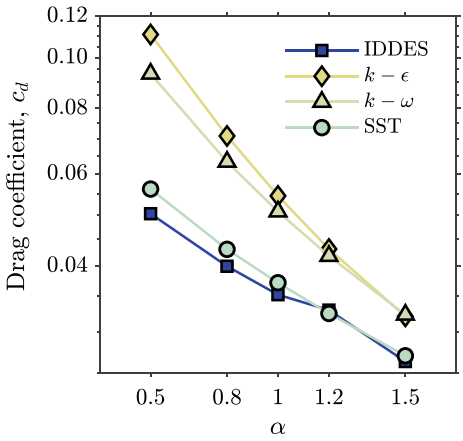


**Fig. 7** Comparison of the drag coefficient predictions by the IDDES and various RANS models along periodic hill walls for the various geometries

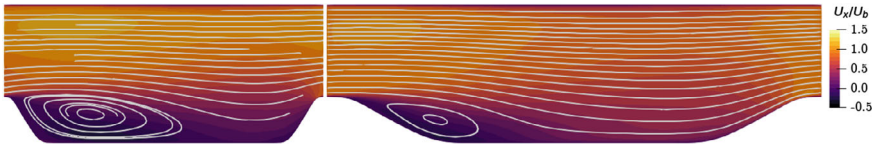


**Fig. 8** Normalised streamwise velocity predictions overlaid by the streamlines from the IDDES simulations for the shape $\alpha = 0.5$ (left), and $\alpha = 1.5$ (right)

Finally, comparisons of the root-mean-squared errors for the IDDES and various RANS-based simulations against the DNS dataset are shown in Fig. 9. For the four quantities considered (streamwise and wall normal velocity component, and the normal and shear stresses), the IDDES results show considerably lower errors compared to the RANS-based predictions. The $k-\omega$ model has a marginally lower error for the streamwise velocity predictions compared to the IDDES results, however, is not consistent in the other three quantities considered.

## 3 Turbulent Mean Flow Reconstruction

In this second half of the paper we use the IDDES data for the baseline shape ($\alpha = 1.0$) to demonstrate RANS-based turbulent mean flow reconstruction using the field inversion approach.

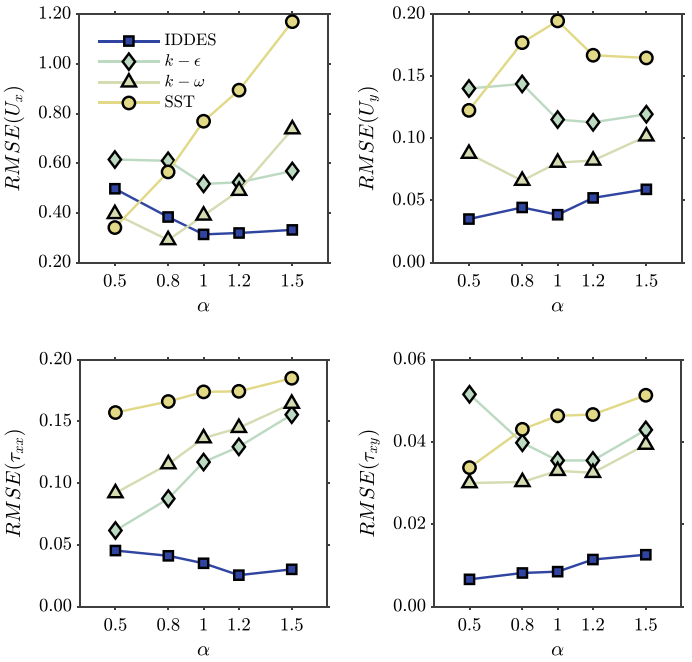


**Fig. 9** Root-mean-squared error comparison of the IDDES results compared to three RANS-based results. $\alpha$, $U_x$, $U_y$, $\tau_{xx}$, $\tau_{xy}$ represent the five periodic hill geometries in Fig. 1, the streamwise and wall-normal velocity components, and the normal and shear Reynolds stresses, respectively

## *3.1 Field Inversion Formulation*

In field inversion the turbulent flow reconstruction is performed by perturbing one of the transport equations in the turbulence model. We use the two-equation $k-\omega$ SST model as the baseline model in this case, and perturb the turbulence dissipation transport equation $\omega$, by a scalar field $\beta_{\text{FI}}$. The transport equation for the turbulence dissipation is thus expressed as follows in the general form:

$$\frac{D\omega}{Dt} = \beta_{\text{FI}}\left(\boldsymbol{x}\right)\mathcal{P}_\omega + \mathcal{T}_\omega - \mathcal{D}_\omega, \tag{2}$$

where $\mathcal{P}$, $\mathcal{T}$, and $\mathcal{D}$ are the production, transport, and dissipation terms of the transport equation, respectively. The baseline model is recovered with $\beta = 1$.

With the goal of reducing the error between the baseline $k-\omega$ SST model and the IDDES data, optimum values for $\beta_{\text{FI}}$ is sought in all the mesh cells by minimising an objective function of the following form:

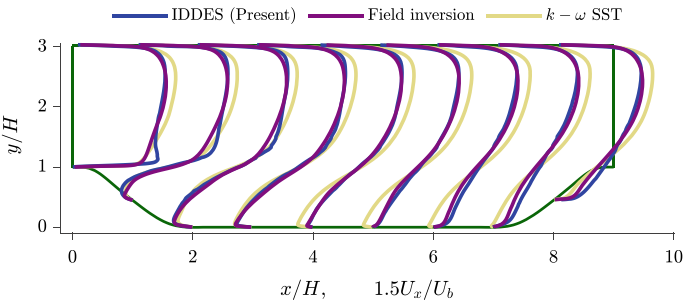


**Fig. 10** Comparison of the streamwise velocity profiles

$$\min_{\beta} \quad \mathcal{J} = \left( \sum_{i=1}^{N_d} w_i \frac{1}{\mathcal{J}_{0,i}} \| \mathcal{G}_i(\beta) - \boldsymbol{d}_i \|_2^2 \right) + \lambda \| \beta - \beta_{\text{prior}} \|_2^2, \tag{3}$$

where $\|.\|_2$ is the $L_2$ norm; the index $i \in \mathbb{R}^{N_d}$ represents the different data quantities (e.g. velocity, and pressure); $\boldsymbol{d}_i$ represents the specific quantity from high-fidelity data, with $\mathcal{G}_i(\beta)$ representing the RANS model equivalent; $w_i$ are the weights; $\mathcal{J}_{0,i}$ are the least-square errors between the baseline model and data; $\lambda$ is a regularisation parameter to avoid an ill-posed optimisation formulation which is set to $10^{-10}$, and $\beta_{\text{prior}}$ is typically assumed to be 1, to bias the solution closer the baseline model. The high fidelity data we use are the streamwise and wall normal velocity fields, and the drag coefficient on the hill wall. This is a multi-objective optimisation problem. In [14] we investigated the effects of different weights $w_i$ for the terms in Eq. (3), and generated a Pareto-optimal front, concluding that equal weighting is appropriate. Therefore, we choose equal weights for all quantities. Due to the high dimensionality of the problem, an adjoint-based optimisation problem is solved, with the implementation documented in [18].

## *3.2 Results*

The streamwise velocity profiles and the lower wall skin friction predictions are shown in Figs. 10 and 11, respectively. The field inversion is able to significantly improve the predictions by the baseline $k-\omega$ SST model. Significant improvements are also achieved in the drag coefficient prediction on the hill wall, and the location of flow reattachment, as shown in Table 1.

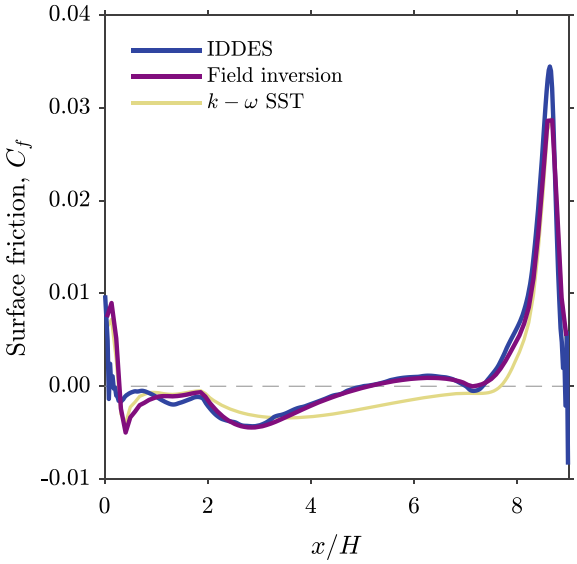


**Fig. 11** Comparison of the skin friction prediction on the hill wall

**Table 1** Drag coefficient and flow reattachment location comparison on the lower wall for the baseline geometry

| Quantity | IDDES | Baseline | Field inversion |
|---|---|---|---|
| $C_d$ | 0.0353 | 0.0372 | 0.0354 |
| $(x/H)_{\text{re-attach.}}$ | 5.02 | 7.68 | 5.12 |

The error reduction in the baseline model after mean flow reconstruction is summarised in Table 2. There are significant reductions in error in most quantities of interest (i.e. velocity prediction, and surface quantities), whereas, the errors in the Reynolds stress predictions are marginally reduced. The latter is in line with results previously reported in literature, where field inversion cannot achieve the same level of error reduction in the Reynolds stress predictions as the other quantities of interest (e.g. [19]).

## 4 Conclusion

We generated and presented turbulent flow simulation results for a set of parameterised periodic hill geometries which involve mild to massive flow separations. The simulations were performed using the improved delayed-detached eddy simulation (IDDES) approach. The IDDES results were compared to reference data from

**Table 2** Root-mean-square comparison of the baseline $k-\omega$ SST and the field inversion predictions with respect to the IDDES data

| Quantity | RMSE Baseline | RMSE field inversion | % error reduction |
|---|---|---|---|
| $U_x$ | 0.8290 | 0.3521 | 57.53 |
| $U_y$ | 0.1765 | 0.1023 | 42.07 |
| $\tau_{xx}$ | 0.1485 | 0.1372 | 7.61 |
| $\tau_{xy}$ | 0.0418 | 0.0394 | 5.57 |
| $C_f$ | 0.0021 | 0.0012 | 42.25 |
| $C_d$ | $1.8749 \times 10^{-3}$ | $0.1190 \times 10^{-3}$ | 93.65 |

$U_x$, $U_y$, $\tau_{xx}$, $\tau_{xy}$, $C_f$, $C_d$ represent the streamwise and wall-normal velocity components, and the normal and shear Reynolds stresses, skin friction and drag coefficient on hill wall, respectively

direct numerical simulations (DNS), and three popular turbulence models—$k-\epsilon$, $k-\omega$, and $k-\omega$ SST—in the context of steady Reynolds-averaged Navier-Stokes (RANS) simulations. IDDES results matched well with the reference DNS data, while all the RANS-based results had varying degrees of discrepancies for the various quantities considered. We then demonstrated turbulent mean flow reconstruction through the adjoint-based field inversion approach to improve the $k-\omega$ SST model. Reconstructed flow results showed significant error reductions in all quantities of interest compared to the original model. Generating high -fidelity datasets using the hybrid RANS-LES approach seems particularly promising for high Reynolds number flows where generating LES or DNS data can be computationally demanding. As mentioned in the introduction, the final goal is to use the generated data for machine-learning-based enhancement of a turbulence model in the context of aerodynamic shape optimisation, which is the subject of our ongoing work.

## Appendix: Spalart-Allmaras IDDES model

The surrogate eddy viscosity $\tilde{\nu}$ is defined as [17]:

$$\frac{\partial \tilde{\nu}}{\partial t} + U_i \frac{\partial \tilde{\nu}}{\partial x_j} = c_{b1}\tilde{S}\tilde{\nu} + \frac{1}{\sigma}\left[\nabla \cdot (\tilde{\nu}\nabla\tilde{\nu}) + c_{b2}\,(\nabla\tilde{\nu})^2\right] - c_{w1} f_w \left(\tilde{r}\left(\frac{\tilde{\nu}}{l_{IDDES}}\right)^2\right), \tag{4}$$

where the turbulent eddy viscosity is defined as $\nu_t = f_{v1}\tilde{\nu}$. The functions $f_{v1}$ and $f_w$ are for near-wall corrections, $\tilde{S}$ is the strain rate tensor, the non-dimensional term $\tilde{r}$ is defined as $\nu_t/(\tilde{S}\kappa^2 d_w^2)$, where $\kappa$ is the von Kármán constant, $d_w$ is the distance from the wall, and $\{\sigma, c_{b1}, c_{b2}, c_{w1}\}$ are model constants. The modified length scale $l_{IDDES}$ is used to switch the transition from the unsteady RANS to scale-resolving LES, and along with the intermediate variables and functions, is defined as:

$$
\begin{aligned}
l_{IDDES} &= \tilde{f}_d\,(1+f_e)\,d_w + (1-\tilde{f}_d) l_{LES},\\
l_{LES} &= C_{DES}\psi\Delta, \quad C_{DES} = 0.65,\\
\Delta &= \min(\max([C_w d_w, C_w h_{max}, h_{wn}])),\\
\tilde{f}_d &= max(1-f_d, f_B),\\
f_d &= 1-\tanh\left[8\left(r_d^3\right)\right],\\
f_B &= \min\left[2\exp\left(-9\alpha^2\right), 1.0\right],\\
\alpha &= 0.25 - \frac{d_w}{h_{max}},\\
f_e &= max\left[(f_{e1}-1), 0\right]\psi f_{e2},
\end{aligned}
\tag{5}
$$

for detailed discussions refer to Shur *et al.* [17].

## References


1. Duraisamy, K., Iaccarino, G., Xiao, H.: Turbulence modeling in the age of data. Annu. Rev. Fluid Mech. **51**, 357–377 (2019)
2. Rowley, C., Dawson, S.: Model reduction for flow analysis and control. Annu. Rev. Fluid Mech. **49**, 387–417 (2017)
3. Cai, S., Mao, Z., Wang, Z., Yin, M., Karniadakis, G.: Physics-informed neural networks (PINNs) for fluid mechanics: a review. Acta. Mech. Sin. **37**, 1727–1738 (2021)
4. Xiao, H., Wu, J., Laizet, S., Duan, L.: Flows over periodic hills of parameterized geometries: a dataset for data-driven turbulence modeling from direct simulations. Comput. Fluids. **200**, 104431 (2020)
5. Breuer, M., Peller, N., Rapp, C., Manhart, M.: Flow over periodic hills-numerical and experimental study in a wide range of Reynolds numbers. Comput. Fluids **38**, 433–457 (2009)
6. Krank, B., Kronbichler, M., Wall, W.: Direct numerical simulation of flow over periodic hills up to $Re_H = 10,595$. Flow Turbul. Combust. **101**, 521–551 (2018)
7. Gloerfelt, X., Cinnella, P.: Large eddy simulation requirements for the flow over periodic hills. Flow Turbul. Combusti. **103**, 55–91 (2019)
8. Ling, J., Kurzawski, A., Templeton, J.: Reynolds averaged turbulence modelling using deep neural networks with embedded invariance. J. Fluid Mech. **807**, 155–166 (2016)
9. Weatheritt, J., Sandberg, R.: The development of algebraic stress models using a novel evolutionary algorithm. Int. J. Heat Fluid Flow **68**, 298–318 (2017)
10. Schmelzer, M., Dwight, R., Cinnella, P.: Discovery of algebraic Reynolds-stress models using sparse symbolic regression. Flow Turbul. Combust. **104**, 579–603 (2020)
11. Xiao, H., Cinnella, P.: Quantification of model uncertainty in RANS simulations: a review. Prog. Aerosp. Sci. **108**, 1–31 (2019)
12. Singh, A., Medida, S., Duraisamy, K.: Machine-learning-augmented predictive modeling of turbulent separated flows over airfoils. AIAA J. **55**, 2215–2227 (2017)
13. Parish, E., Duraisamy, K.: A paradigm for data-driven predictive modeling using field inversion and machine learning. J. Comput. Phys. **305**, 758–774 (2016)
14. Bidar, O., He, P., Anderson, S., Qin, N.: Turbulent mean flow reconstruction based on sparse multi-sensor data and adjoint-based field inversion. AIAA AVIATION 2022 Forum (2022)
15. Fröhlich, J., Terzi, D.: Hybrid LES/RANS methods for the simulation of turbulent flows. Prog. Aerosp. Sci. **44**, 349–377 (2008)
16. Chaouat, B.: The state of the art of hybrid RANS/LES modeling for the simulation of turbulent flows. Flow Turbul. Combust. **99**, 279–327 (2017)

17. Shur, M., Spalart, P., Strelets, M., Travin, A.: A hybrid RANS-LES approach with delayed-DES and wall-modelled LES capabilities. Int. J. Heat Fluid Flow **29**, 1638–1649 (2008)
18. Bidar, O., He, P., Anderson, S., Qin, N.: An open-source adjoint-based field inversion tool for data-driven RANS modelling. AIAA AVIATION 2022 Forum (2022)
19. Singh, A., Duraisamy, K., Zhang, Z.: Augmentation of turbulence models using field inversion and machine learning. 55th AIAA Aerosp. Sci. Meet. p. 0993 (2017)
20. Menter, F., Kuntz, M., Langtry, R.: Ten years of industrial experience with the SST turbulence model. Turbul. Heat Mass Transf. **4**, 625–632 (2003)
21. Balakumar, P., Park, G.: DNS/LES simulations of separated flows at high reynolds numbers. 45th AIAA fluid dynamics conference (2015)
22. Frohlich, J., Mellen, C.P., Rodi, W., Temmerman, L., Leschziner, M.A.: Highly resolved large-eddy simulation of separated flow in a channel with streamwise periodic constrictions. J. Fluid Mech. **526**, 19–66 (2005)
23. Heinz, S., Mokhtarpoor, R., Stoellinger, M.: Theory-based reynolds-averaged navier-stokes equations with large eddy simulation capability for separated turbulent flow simulations. Phys. Fluids. **32**, (2020)
24. Wilcox, D.: Turbulence modeling for CFD. DCW industries La Canada, CA (1998)
25. Launder, B., Spalding, D.: The numerical computation of turbulent flows, pp. 96–116. Numerical Prediction Of Flow, Heat Transfer, Turbulence And Combustion (1983)
26. Jasak, H., Jemcov, A., Tukovic, Z.: OpenFOAM: A C++ library for complex physics simulations. International workshop on coupled methods in numerical dynamics. pp. 1–20 (2007)
27. Travin, A., Shur, M., Strelets, M., Spalart, P.: Physical and numerical upgrades in the detached-eddy simulation of complex turbulent flows. Adv. LES Complex Flows. pp. 239–254 (2002)
28. Robertson, E., Choudhury, V., Bhushan, S., Walters, D.: Validation of OpenFOAM numerical methods and turbulence models for incompressible bluff body flows. Comput. Fluids **123**, 122–145 (2015)
29. Saini, R., Karimi, N., Duan, L., Sadiki, A., Mehdizadeh, A.: Effects of near wall modeling in the improved-delayed-detached-eddy-simulation (IDDES) methodology. Entropy **20**, 771 (2018)
30. Chaouat, B., Schiestel, R.: Hybrid RANS/LES simulations of the turbulent flow over periodic hills at high Reynolds number using the PITM method. Comput. Fluids **84**, 279–300 (2013)
31. Heinz, S., Mokhtarpoor, R., Stoellinger, M.: Hybrid RANS-LES periodic hill flow simulations up to extreme reynolds numbers. AIAA Scitech 2021 Forum (2021)
32. Rapp, C., Manhart, M.: Flow over periodic hills: an experimental study. Exp. Fluids **51**, 247–269 (2011)